



Figure 1. We present ODYSSEY, a unified mobile manipulation framework for agile quadruped robots equipped with manipulators, which seamlessly integrates high-level task planning with low-level whole-body control.

Abstract

Language-guided long-horizon mobile manipulation has long been a grand challenge in embodied semantic reasoning, generalizable manipulation, and adaptive locomotion. Three fundamental limitations hinder progress: First, although large language models have shown promise in enhancing spatial reasoning and task planning through learned semantic priors, existing implementations remain confined to tabletop scenarios, failing to address the constrained perception and limited actuation ranges characteristic of mobile platforms. Second, current manipulation strategies exhibit insufficient generalization when confronted with the diverse object configurations encountered in open-world environments. Third, while crucial for practical deployment, the dual requirement of maintaining high platform maneuverability alongside precise end-effector control in unstructured settings remains un-

derstudied in the literature.

In this work, we present ODYSSEY, a unified mobile manipulation framework for agile quadruped robots equipped with manipulators, which seamlessly integrates high-level task planning with low-level whole-body control. To address the challenge of egocentric perception in language-conditioned tasks, we introduce a hierarchical planner powered by a vision-language model, enabling long-horizon instruction decomposition and precise action execution. At the control level, our novel whole-body policy achieves robust coordination of locomotion and manipulation across challenging terrains. We further present the first comprehensive benchmark for long-horizon mobile manipulation, evaluating diverse indoor and outdoor scenarios. Through successful sim-to-real transfer, we demonstrate the system's generalization and robustness in real-world deployments, underscoring the practicality of legged manipulators in unstructured environments. Our work advances the feasibility of generalized robotic assistants capable of complex, dynamic tasks. Our

*These authors contributed equally.

†Corresponding authors.

1 Introduction

Open-world mobile manipulation allows robots to autonomously navigate and interact in dynamic, unstructured environments by tightly integrating mobility, manipulation, and real-time perception. Unlike traditional methods that separate navigation and manipulation, this unified approach unlocks emergent capabilities like active perception, which is essential for real-world tasks. For example, a robot might subtly adjust its position while reaching for an object to gain a better grasp position. This adaptive behavior emerges naturally in complex environments where static perception or sequential planning would fail.

Prior research has achieved robust solutions for navigation in dynamic environments (Grandia et al. 2023; Zhuang et al. 2023; Liu et al. 2024b) and manipulation in controlled settings (Kim et al. 2024; Brohan et al. 2022; Cheang et al. 2024). While recent works (Pan et al. 2025a; Fu, Cheng, and Pathak 2023; Liu et al. 2024a; Zhang et al. 2025; Wang et al. 2024b) have developed whole-body control frameworks, they face scalability limitations in open-world scenarios due to simplified environmental assumptions and evaluations restricted to short-horizon tasks. We present ODYSSEY, a reinforcement learning-based whole-body control system that unifies robust quadruped locomotion with precise manipulation through an integrated vision-language framework. Our approach achieves state-of-the-art control accuracy under out-of-distribution conditions while significantly expanding operational capabilities. Unlike prior work, we demonstrate generalization across diverse challenging terrains, enabling real-world deployment.

Recent works (Qi et al. 2025; Pan et al. 2025b) demonstrate that large language models can substantially enhance robotic task planning and generalizable manipulation through their spatial understanding abilities. We extend the capability of large language models to whole-body navigation and manipulation tasks. Specifically, our approach grounds task execution at two levels: task-level planning over a semantic instance map and fine-grained action guidance via geometry-constrained pose estimation.

Besides, to address the critical evaluation gap, we present the first comprehensive benchmark for evaluating long-horizon mobile manipulation, featuring eight diverse daily tasks across indoor/outdoor environments with hundreds of object configurations. The benchmark enables holistic assessment of embodied reasoning, task planning, navigation, and manipulation capabilities, while incorporating the standardized Arnold framework for precise manipulation evaluation.

Through extensive experiments, our system shows strong ability for sim2real transfer, showcasing exceptional generalization where both control and planning modules maintain consistent performance across diverse real-world scenarios. Our contributions are four folds:

(i) We introduce a hierarchical vision-language planner that bridges egocentric perception and language-conditioned

tasks, decomposing long-horizon instructions into executable actions.

(ii) We propose the first whole-body control policy that generalizes to challenging terrains while jointly coordinating locomobility and manipulation.

(iii) We introduce the first long-horizon mobile manipulation benchmark, covering a wide range of realistic indoor and outdoor scenarios.

(iv) We further demonstrate successful sim-to-real transfer of both high-level planners and low-level control policies, showing strong generalization and robustness in real-world deployments.

Our results highlight the feasibility and practicality of deploying a legged mobile manipulator in unstructured environments, paving the way toward generalized robotic assistants.

2 Related Work

2.1 Open-world mobile manipulation

Previous research has made significant advances in both navigation and manipulation as separate domains, with robust solutions developed for mobile robot path planning in dynamic environments (Grandia et al. 2023; Zhuang et al. 2023) and sophisticated manipulation techniques for object interaction in controlled settings (Kim et al. 2024; Brohan et al. 2022; Cheang et al. 2024). While pioneering works (Pan et al. 2025a; Fu, Cheng, and Pathak 2023; Liu et al. 2024a; Zhang et al. 2025; Wang et al. 2024b; Fu, Zhao, and Finn 2024; Jiang et al. 2025b) have developed initial whole-body control frameworks, they face scalability limitations in open-world scenarios due to oversimplified environmental assumptions and evaluations limited to short-horizon pick-and-place tasks. Some works (Ha et al. 2024; Qiu et al. 2024b) have attempted to attach more complex interactions by learning per-action policies from human demonstrations. However, these methods lack compositionality and scalability, needing task-specific data for each scenario. ODYSSEY overcomes these limitations by unifying terrain-aware locomotion with hierarchical planning, enabling robust mobile manipulation in unstructured environments.

2.2 Foundation Models for Embodied Tasks

Vision-language models (VLMs) have shown promise in enhancing robotic reasoning (Qi et al. 2025; Pan et al. 2025b; Zhi et al. 2024; Qiu et al. 2024a; Wang et al. 2025), but their evaluation has been restricted to tabletop settings with fixed cameras. For navigation, foundation models improve spatial understanding (Gu et al. 2024; Jatavallabhula et al. 2023; Jiang et al. 2025a), yet they lack fine-grained manipulation support. ODYSSEY advances this by grounding hierarchical planning in egocentric perception, using VLMs to decompose tasks via scene graphs while generating precise end-effector trajectories. This contrasts with modular approaches (Zhang et al. 2025) that struggle with compositional reasoning under uncertainty.

2.3 Benchmarks for Real-World Deployment

Existing benchmarks for mobile manipulation (Qiu et al. 2024a) focus narrowly on navigation or short-term interactions, lacking standardized metrics for long-horizon tasks. Simulation frameworks like IsaacSim have enabled progress in locomotion (Zhi et al. 2024), but manipulation-centric evaluations remain sparse. ODYSSEY introduces a comprehensive benchmark with diverse indoor/outdoor scenarios, addressing multi-stage reasoning, object-aware navigation, and precision manipulation. This complements prior work (Qiu et al. 2024b) by enabling scalable testing of sim-to-real transfer for integrated control and planning.

3 Method

In this section, we present ODYSSEY, a unified framework that spans long-horizon task planning, whole-body control, and standardized evaluation for mobile manipulation. It comprises three key components:

1. **Coarse-to-Fine Task Planner** (Section 3.1): a hierarchical planner that orchestrates top-down task execution under the guidance of foundation models.
2. **Quadruped Whole-Body Policy** (Section 3.2): a reinforcement learning-based whole-body controller that generalizes to diverse terrains and overcomes sim-to-real gap.
3. **Mobile Manipulation Benchmark** (Section 3.3): the first scalable evaluation suite for assessing long-term task performance across versatile real-world scenarios.

3.1 Long-horizon Task Planner

To bridge the gap left by prior work in modeling the intricate dependencies between semantic reasoning-based navigation and fine-grained, generalizable manipulation, our hierarchical framework is explicitly designed to ensure the reliability of both components while reinforcing their mutual dependencies for coherent long-horizon task execution.

Map-Aware Task-Level Planning To support long-horizon task planning grounded in egocentric observations, we first build a global planner that integrates a lightweight multi-modal perception module as a plug-in component. Concretely, we fuse on-board RGB and LiDAR streams to form a unified spatial-semantic representation of the scene. Leveraging a suite of pre-trained foundation models, we map an instance graph that encodes object geometry and semantics for symbolic task reasoning. The pipeline of this module is detailed in Appendix A.1.

As illustrated in Fig. 2, given the instance-level semantic map, GPT-4.1 (Achiam et al. 2023) is used to break down template-free natural language instructions into a sequence of atomic actions from a predefined set: `navigate`, `pick`, `place`, and `push/pull/drag`. Each action is paired with a language description that tracks task progress and provides guidance for local planning.

For actions involving spatial displacement (`navigate`, `drag`), the model is further prompted to output a coarse target waypoint to guide planning. We project this target

onto a 2D occupancy map built via online SLAM from accumulated LiDAR scans. A local search is then performed around the projected waypoint to identify a collision-free goal pose, avoiding object bounding boxes and structural obstacles. This process yields a globally grounded task plan that aligns with the scene context and is feasible under physical constraints.

Geometry-Constrained Local Manipulation For atomic actions requiring close-range manipulation, we use wrist-mounted depth observations to guide a vision-language model for precise end-effector pose generation. Despite the diverse physical nature of different actions, we unify their execution through a single visuomotor interface, eliminating the need for per-action heuristics.

Specifically, given an RGB observation and the corresponding textual description of the current atomic action, we employ Qwen2.5-VL-72B-Instruct (Bai et al. 2025), a model enhanced with pixel-level grounding capabilities, to infer a task-relevant contact point $p^* \in \mathbb{R}^2$ in the image space.

The contact point is projected onto the aligned depth image to recover its corresponding 3D position in the robot coordinate frame, denoted as $\mathbf{P}_{ee} \in \mathbb{R}^3$. We further prompt the model to generate the orientation $\mathbf{R}_{ee} \in SO(3)$ of the end-effector by determining the gripper’s closing direction(x -axis) and approaching direction(z -axis), subject to the following geometric constraints:

- **Axis-alignment constraint:** When the target object or contact region exhibits a dominant axis $\mathbf{a} \in \mathbb{R}^3$, both the x -axis and z -axis of the end-effector should be orthogonal to it:

$$\mathbf{r}_x^\top \mathbf{a} = 0, \quad \mathbf{r}_z^\top \mathbf{a} = 0. \quad (1)$$

- **Surface-normal constraint:** If the object is attached to a planar surface with normal vector $\mathbf{n} \in \mathbb{R}^3$, then the z -axis of the end-effector should align with the surface normal without violating the first constraint:

$$\mathbf{r}_z \parallel \mathbf{n}, \quad \text{s.t.} \quad \mathbf{r}_z^\top \mathbf{a} = 0. \quad (2)$$

By leveraging the expressive grounding capacity of Qwen-VL and constraining the output pose with interpretable geometric conditions, our system achieves reliable local guidance for interaction-intensive manipulation primitives. To the best of our knowledge, this constitutes the first fine-grained manipulation planning system without third-person observation or scripted policies, marking a significant step toward scalable deployment in mobile, in-the-wild environments.

3.2 Policy for Whole-body Control

To effectively execute commands from a high-level planner and adapt to diverse terrains, a whole-body control policy is essential. This work proposes a two-stage, learning-based policy that utilizes a neural network to generate desired joint positions from a set of observations. To enhance the policy’s robustness, the training process incorporates a carefully designed, terrain-invariant end-effector sampling strategy and

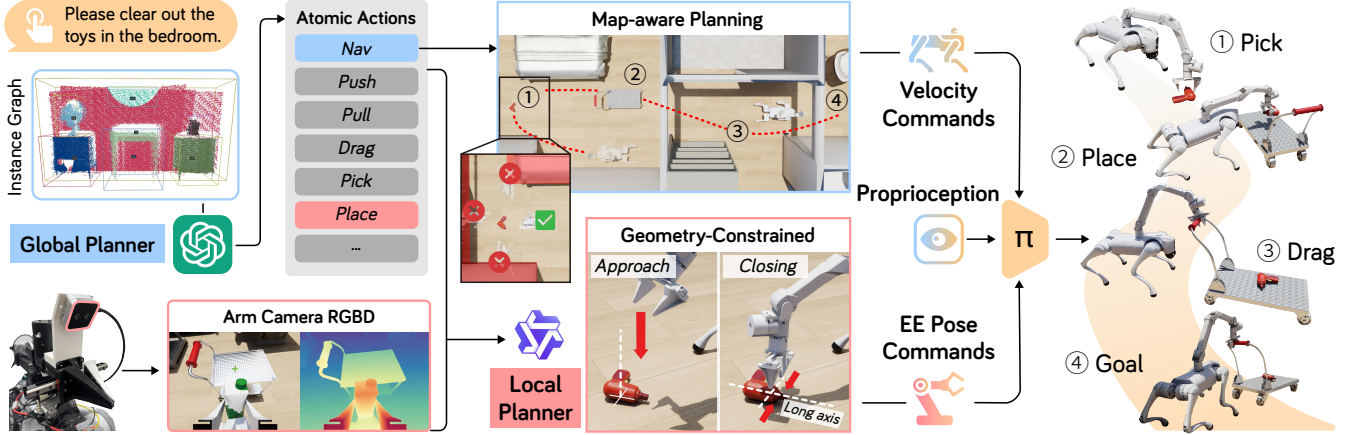


Figure 2: ODYSSEY pipeline spans the entire process of a long-horizon task, including multi-modal semantic perception, map-aware global planning, geometry-constrained action grounding, and step-wise execution by a learned low-level policy.

comprehensive domain randomization. The resulting controller is resilient to varied environmental interactions and can be directly deployed on a physical robot. This section first defines the policy and subsequently discusses the training methodology.

Mobile Manipulation Policy The mobile manipulation policy π is formulated as a single network that maps a comprehensive observation vector to a target action $\mathbf{a}_t \in \mathbb{R}^{18}$ as shown in Eq.4. The observation includes the locomotive command $\mathbf{c}_t = (\hat{x}, \hat{y}, \hat{\omega})$, the 6-D end-effector target \mathbf{e}_t , a local ground height map \mathbf{m}_t , the projected gravity vector \mathbf{g}_t , the previous timestep $\mathbf{a}_{t-1} \in \mathbb{R}^{18}$ and the proprioceptive state $\mathbf{s}_t \in \mathbb{R}^{36}$ (joint positions \mathbf{q}_t and velocities $\dot{\mathbf{q}}_t$). All commands and targets are expressed in the robot’s base frame. To stabilize the policy output and reduce the simulation-to-reality gap (Fu, Cheng, and Pathak 2023), the action \mathbf{a}_t is formulated as the offsets to the default joint configuration $\mathbf{q}^{default} \in \mathbb{R}^{18}$. The final target, $\mathbf{q}_t^{target} = \mathbf{q}^{default} + \mathbf{a}_t$, is then converted to torques by a Proportional-Derivative (PD) controller.

$$\mathbf{s}_t = (\mathbf{q}_t, \dot{\mathbf{q}}_t) \quad (3)$$

$$\mathbf{a}_t = \pi(\mathbf{c}_t, \mathbf{e}_t, \mathbf{s}_t, \mathbf{g}_t, \mathbf{m}_t, \mathbf{a}_{t-1}) \quad (4)$$

To enhance training robustness and avoid local minima associated with searching a large action space, we employ a two-stage curriculum learning approach, as shown in Fig. 3. **Stage 1** In this stage, the arm joints are fixed to focus training on locomotion under a static load, improving exploration efficiency. Inspired by (Mittal et al. 2023), we introduce a gait reward incorporated alongside the base tracking reward to structure the robot’s gait. Furthermore, a novel frequency reward is introduced to regulate the gait’s cadence. The gait reward r_{gait} encourages specific synchronous (e.g., diagonal) and asynchronous (e.g., lateral) foot contact patterns, with reward functions r_s and r_a detailed in the Appendix B.1.

$$r_{gait} = \prod_{i,j \in \text{sync pairs}} r_s(i,j) \cdot \prod_{k,l \in \text{async pairs}} r_a(k,l) \quad (5)$$

The frequency reward r_{fre} regulates the gait’s cadence based on the error from a target frequency f_{target} . The gait frequency $f(\text{leg})$ is the inverse of the time between consecutive ground contacts ($t_k^{cont} - t_{k-1}^{cont}$). The reward is then:

$$err(\text{leg}) = (f(\text{leg}) - f_{target})^2 \quad (6)$$

$$r_f(\text{leg}) = \exp(-0.5 \cdot err(\text{leg})) \quad (7)$$

$$r_{fre} = \prod_{\text{leg} \in \text{FL,FR,RL,RR}} r_f(\text{leg}) \quad (8)$$

Stage 2 Following 2k training iterations, the process transitions to the second stage. In this stage, the policy controls all 18 joints, encompassing both the manipulator and the four legs. Consequently, the reward function is expanded to include end-effector tracking terms, r_{arm} , in addition to the previously described locomotion rewards, to guide the policy’s training.

Terrain-Invariant End-Effector Sampling To ensure robust performance across varied topographies, our method employs a terrain-invariant end-effector sampling strategy. The process begins by sampling a target position from a spherical volume defined in the world coordinate system, centered at the robot’s arm base. A key aspect of this strategy is that the target’s z-axis height is fixed within the world frame before the coordinates are transformed into a Cartesian target position relative to the robot’s moving base frame. This approach offers a significant advantage over sampling directly in the arm’s local frame, as it effectively decouples the end-effector target from disturbances caused by changes in the robot’s base pitch or the underlying terrain height. Consequently, this decoupling improves interaction accuracy during task execution.

Domain Randomization To bridge the simulation-to-reality gap, domain randomization is employed throughout the training process, a strategy supported by recent research (Fu, Cheng, and Pathak 2023; Pan et al. 2025a). To ensure adaptability to different payloads, the end-effector’s mass is also randomized during training, improving the policy’s ability to handle objects of unknown weight. A detailed

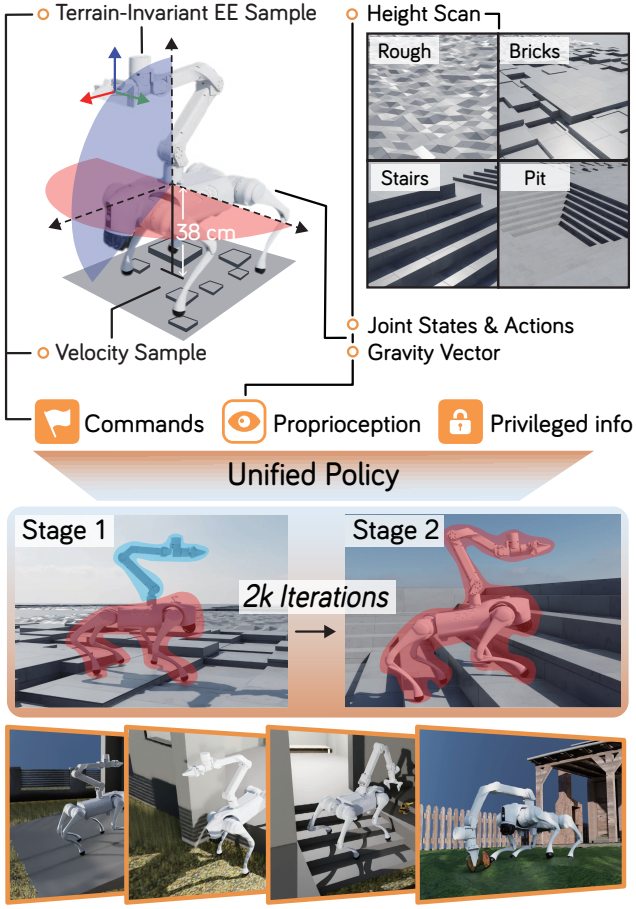


Figure 3: An overview of the mobile manipulator policy and its two-stage training framework.

breakdown of all randomization parameters and the key reward components is provided in the Appendix B.2.

3.3 Simulation Benchmark

To evaluate navigation, manipulation, and whole-body control as a unified system, we present the first simulation benchmark tailored for long-horizon mobile manipulation in both indoor and outdoor environments.

Asset and Scene Library To support realistic and versatile evaluation environments, we curate a diverse set of assets encompassing both object instances and full-scale 3D scenes. The object assets are sourced from a combination of prior open-source datasets (Wang et al. 2024a; Team 2025; Nasiriany et al. 2024), publicly available object repositories, and manually created models.

Object Assets: We curate a diverse set of interactive objects categorized into four types: 50 rigid objects (e.g., common graspable items), 15 containers (e.g., bowls and bins with annotated containment region), 30 articulated structures (e.g., cabinets and doors), and 10 drappable items (e.g., carts and chairs).

Environments: Our benchmark includes 10 realistic

scenes, with 5 indoor homes, 2 supermarkets, 1 restaurant, and 2 outdoor courtyards featuring slopes and stairs. All environments are designed for full traversability by legged robots and support multiple initialization zones to allow sampling and spatial variation of large-scale tasks.

Rich Domain-style Variation To ensure generalization, we incorporate variability across four dimensions during simulation rollout: (1) *Object layouts* are varied within semantic constraints across episodes, promoting diversity in interaction. (2) *Physical attributes*, including mass, friction, and articulation limits, are resampled per episode to induce dynamic variability. (3) *Environment conditions* such as lighting, material textures, and clutter elements are randomized to simulate perceptual noise. (4) *Terrain complexity* is varied across outdoor scenes to assess locomotion robustness.

Multi-stage Task Suite Our benchmark includes two categories of tasks: short-horizon manipulation skills merged from ARNOLD (Gong et al. 2023), and long-horizon mobile manipulation tasks designed to reflect practical daily scenarios.

Short-Horizon Arnold Tasks. We integrate four single-step manipulation tasks from the ARNOLD benchmark: PICKUPOBJECT, REORIENTOBJECT, OPENCABINET, and CLOSECABINET. While retaining their original goal state definitions and scene configurations, we adjust the spatial layout and object positioning to accommodate the kinematics and workspace of our quadruped robot platform, ensuring fair and consistent evaluation.

Long-Horizon Mobile Manipulation. To assess the system’s embodied reasoning, navigation, and sequential manipulation capabilities, we construct 8 multi-stage tasks spanning diverse indoor and outdoor scenarios. Each task consists of 2–3 subgoals, with a total of 246 indoor and 58 outdoor variations spanning object types, spatial layouts, and interaction modes.

Our task pool emphasizes a broad range of skills spanning grasping, reorientation, container placement, articulated manipulation, and long-term navigation over complex terrain. The combination of short and long-horizon tasks enables benchmarking at both low-level manipulation and high-level planning. Detailed task configurations are elaborated in Appendix C.

Modular Evaluation Protocol We evaluate both overall task success and per-action success rate. For instance, in the CARTDELIVERY task, we define subtasks such as *nav_to_object*, *pick_object*, *nav_to_cart*, *place_object*, *drag_cart*, and *nav_to_goal*. We determine actions success by monitoring the robot and cart’s world poses, as well as the relative pose between the object and the cart. A subtask is considered complete if its corresponding goal condition is met during the task horizon. This protocol captures both execution precision and planning consistency.

4 Experiment

4.1 High-level Planner Performance

To evaluate the performance of our high-level planner in a modular and scalable manner, we conducted experiments based on the benchmark discussed in Section 3.3. Firstly, we tested our local planner on thousands of single-step test cases, focusing on precision and consistency. Secondly, we integrated the global planner and evaluated our proposed approach on several hundred long-horizon mobile manipulation tasks. Additionally, we performed a detailed analysis of the completion rates for the decomposed atomic actions within each task.

ARNOLD Short-horizon Tasks Before moving on to the long-horizon evaluation, we first conducted experiments in relatively confined spaces to demonstrate the fine-grained operation precision and generalization capabilities of our framework. We migrated four short-horizon tasks from ARNOLD and faithfully replicated their continuous monitoring system for goal states.

Their evaluation protocol divides five splits into two categories: 1) *Seen* includes shuffled seen data; 2) *Novel* features one of unseen components (objects, scenes, or goal states). We compare against their strongest baseline model PerAct (Shridhar, Manuelli, and Fox 2022), an end-to-end imitation learning paradigm trained on large-scale human trajectories, which leverages observations from five external cameras to achieve accurate spatial perception. As shown in Table 1, our method achieves substantial overall improvements, demonstrating superior fine-grained manipulation capabilities while relying solely on a single egocentric camera. Moreover, while their performance declined dramatically on novel splits, our method maintains stable performance across all datasets, showcasing generalized ability to handle O.O.D object configurations. Further experiment details are provided in Appendix D.1.

	Seen		Novel	
	PerAct	Ours	PerAct	Ours
P.OBJECT	94.03	60.45	25.70	45.24
R.OBJECT	19.48	51.32	8.23	52.09
O.CABINET	31.09	56.30	16.62	51.09
C.CABINET	60.81	74.32	41.32	79.50

Table 1: Performance comparison between our approach and PerAct on 4 ARNOLD tasks, evaluated on both seen and generalized splits by success rate (%).

ODYSSEY Long-horizon Tasks Table 2 summarizes the performance of our system across eight long-horizon mobile manipulation tasks, reporting both overall task success rates and success rates for decomposed atomic actions. Notably, ODYSSEY consistently achieves 40% or higher overall success across all tasks, and maintains over 60% success in each atomic skill category, demonstrating robust coordination in a generalized long-horizon task. Building on this, we highlight several key findings from different perspectives of system performance:

Low-level ability: The consistent success rates across indoor and outdoor settings, despite the presence of irregular terrains, validate the reliable locomotion and effective pose tracking enabled by our terrain-adaptive whole-body control policy. Most control-related failures are caused by interactions with objects positioned beyond the robot’s reachable range.

Fine-grained action: VLM-guided grounding enables high pick and place success rates across all tasks, demonstrating strong capability in identifying and localizing semantic targets. A large portion of failures stem from suboptimal gripper alignment, indicating limitations in the model’s spatial reasoning over object geometry. In addition, tasks involving more complex interactions such as drag and pull occasionally fail due to inaccurate localization, particularly with slim handles or partially occluded items.

Task-level planning: Our global task planner demonstrates strong symbolic reasoning over instance graphs, enabling reliable multi-stage task decomposition. In conjunction, our SLAM-based path planner ensures safe and consistent navigation. These components together lead to high navigate success rates across all tasks.

4.2 Low-level Policy Performance

We evaluated the proposed whole-body control policy against RoboDuet (Pan et al. 2025a), a baseline that also uses a two-stage training process. In contrast to RoboDuet’s dual-policy (locomotion and manipulation) approach with base-centric sampling, our method employs a single, unified policy trained with a novel terrain-invariant end-effector sampling strategy. For the evaluation, 4096 parallel agents were instantiated with five data samples collected from each agent.

Metric To quantitatively evaluate performance in the simulator, the following metrics are defined:

- **Base Tracking Error:** The error between commanded and actual base velocities, comprising linear (e_x, e_y) and angular e_ω components.
- **End-Effector Position Error:** The Euclidean distance (D_{pos}) between the current and commanded end-effector positions in the world frame.
- **End-Effector Orientation Error:** The quaternion geodesic distance (D_{ori}) between the current \mathbf{q}_{curr} and target \mathbf{q}_{tar} orientations, calculated as $D_{ori} = 2 * \arccos(|\mathbf{q}_{curr} \cdot \mathbf{q}_{tar}|)$.

Simulation result Our method was compared with evaluations conducted under both static (standing) and dynamic (moving) conditions. Due to the robot’s structural constraints, sampling unreachable samples leads to self-collisions, which negatively impact the training process. To mitigate this issue, we deliberately reduced the volume of the sampling space used during training. To ensure a fair comparison and test generalization, both methods were evaluated in the same, larger workspace, as detailed in Table 4, with the comparative results of this evaluation presented in Table 3.

	I.COLLECT	R.NAVIGATE	C.DELIVERY	C.STORAGE	RESTOCKING	SHOPPING	O.COLLECT	O.DELIVERY
Navigate	97.4	86.6	98.3	97.7	98.2	98.3	98.4	95.6
Pick	72.7	/	84.6	79.6	83.3	85.0	69.0	72.7
Place	96.8	/	72.7	83.8	79.2	76.5	95.0	80.0
Push/Pull	/	94.1	/	71.0	/	/	/	85.7
Drag	/	/	69.2	/	/	79.2	/	/
Overall	66.7	69.8	41.0	44.9	56.7	47.5	63.3	46.4

Table 2: Overall success rates (%) of 8 ODYSSEY long-horizon tasks, along with per-action success rates for each task.

	Stand still		Move	
	Roboduet	ours	Roboduet	Ours
$e_x \downarrow$	0.32	0.08	9.70	0.36
$e_y \downarrow$	0.34	2.69	15.42	2.31
$e_\omega \downarrow$	0.32	0.26	60.59	0.79
$D_{pos} \downarrow$	11.08	11.48	10.75	10.57
$D_{ori} \downarrow$	47.14	46.93	47.53	47.15

Table 3: The quantitative result under static (stand still) and dynamic (move) conditions.

	Train	Evaluation
	RoboDuet	Ours
\hat{x}	[-1.00, 1.00]	[-1.00, 1.00]
\hat{y}	[0.00, 0.00]	[-1.00, 1.00]
\hat{w}	[-0.60, 0.60]	[-1.00, 1.00]
\hat{l}_{ee}	[0.30, 0.70]	[0.30, 0.65]
\hat{p}_{ee}	[-0.45 π , 0.45 π]	[-0.17 π , 0.33 π]
\hat{y}_{ee}	[-0.50 π , 0.50 π]	[-0.33 π , 0.33 π]
$\hat{\alpha}_{ee}$	[-0.45 π , 0.45 π]	[-0.50 π , 0.50 π]
$\hat{\beta}_{ee}$	[-0.33 π , 0.33 π]	[-0.17 π , 0.50 π]
$\hat{\gamma}_{ee}$	[-0.42 π , 0.42 π]	[-0.50 π , 0.50 π]

Table 4: Sampling ranges for commands used during training and evaluation. The locomotion commands consist of linear velocities (\hat{x} , \hat{y}) and angular velocity (\hat{w}). The end-effector target is defined by a position in spherical coordinates (radius \hat{l}_{ee} , pitch \hat{p}_{ee} and yaw \hat{y}_{ee}) and an orientation in Euler angles ($\hat{\alpha}_{ee}$, $\hat{\beta}_{ee}$, $\hat{\gamma}_{ee}$).

The evaluation results indicate that our policy achieves better performance in base velocity tracking (rows 1-3), an improvement we attribute to the inclusion of terrain data in the policy’s observation, which enhances the robot’s state estimation. End-effector pose tracking performance remains comparable to the baseline (rows 4-5). Notably, a key aspect of this evaluation is that our policy was trained in an end-effector workspace intentionally smaller than that used for the baseline, and our policy is adaptive to different topographies (e.g., steps). This demonstrates strong generalization capabilities from a more constrained training domain of our approach.

4.3 Sim-to-real Performance

We conducted real-world experiments to validate the sim-to-real performance of our framework, which integrates the high-level coarse-to-fine task planner with the low-level whole-body control policy.

Robot System Setup Our robot platform, as shown in Fig. 4, combines a 12-DoF Unitree Go2 quadruped with a 6-DoF Arx5 manipulator. The Go2 (15kg weight, 8kg payload) includes a built-in Unitree L1 LiDAR, and the 3.35kg Arx5 arm is mounted on its back, similar to (Ha et al. 2024). For high-level perception, the platform is equipped with a MID-360 LiDAR for localization and two RealSense cameras: a head-mounted D435i for RGB imagery and a gripper-mounted D405 for RGB-D data. The control policy operates at 50 Hz, with a PD controller issuing motor commands at 200 Hz.

Real-world experiments The ODYSSEY framework was evaluated on two long-term tasks (“navigate to pick” and “pick and place”) using five different objects. The entire system demonstrated successful sim-to-real transfer on task planning and execution as illusion in Fig. 4.

Despite this success, some sim-to-real gaps persist. For instance, the robot occasionally failed at grasping small objects due to the inaccuracies in end-effector tracking and visual perception. Through these experiments, our approach has demonstrated significant potential for solving long-horizon mobile exploration and manipulation tasks, while simultaneously identifying the primary challenges—robust perception and high-precision control—that must be addressed for seamless real-world deployment.

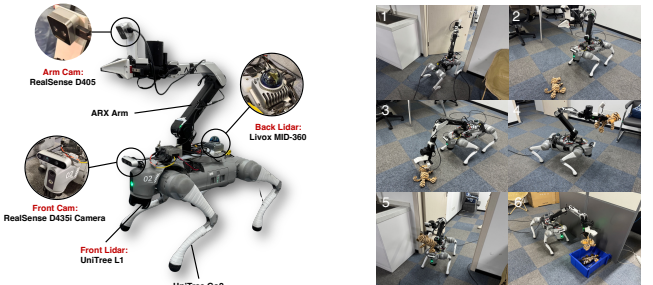


Figure 4: The robot system and real-world experiments

5 Conclusions and Future Work

We present ODYSSEY, a unified framework for open-world mobile manipulation that integrates hierarchical task planning with terrain-adaptive whole-body control. Our approach demonstrates robust sim-to-real transfer and generalization across diverse environments and long-horizon tasks. Future work will extend our benchmark into a comprehensive evaluation paradigm for vision-language models (VLMs) and mobile manipulators, enabling cross-embodiment assessment of semantic reasoning and locomotion-manipulation coordination. Additionally, we aim to explore the emergent capabilities of active perception, where dynamic scene understanding and adaptive motion synergize for more efficient real-world interaction. This direction could unlock new behaviors in cluttered, unstructured environments, further bridging the gap between high-level planning and low-level control.

References

Achiam, J.; Adler, S.; Agarwal, S.; Ahmad, L.; Akkaya, I.; Aleman, F. L.; Almeida, D.; Altenschmidt, J.; Altman, S.; Anadkat, S.; et al. 2023. Gpt-4 technical report. *arXiv preprint arXiv:2303.08774*.

Bai, S.; Chen, K.; Liu, X.; Wang, J.; Ge, W.; Song, S.; Dang, K.; Wang, P.; Wang, S.; Tang, J.; et al. 2025. Qwen2. 5-vl technical report. *arXiv preprint arXiv:2502.13923*.

Brohan, A.; Brown, N.; Carbajal, J.; Chebotar, Y.; Dabis, J.; Finn, C.; Gopalakrishnan, K.; Hausman, K.; Herzog, A.; Hsu, J.; et al. 2022. Rt-1: Robotics transformer for real-world control at scale. *arXiv preprint arXiv:2212.06817*.

Cheang, C.-L.; Chen, G.; Jing, Y.; Kong, T.; Li, H.; Li, Y.; Liu, Y.; Wu, H.; Xu, J.; Yang, Y.; et al. 2024. Gr-2: A generative video-language-action model with web-scale knowledge for robot manipulation. *arXiv preprint arXiv:2410.06158*.

Fu, Z.; Cheng, X.; and Pathak, D. 2023. Deep whole-body control: learning a unified policy for manipulation and locomotion. In *Conference on Robot Learning*, 138–149. PMLR.

Fu, Z.; Zhao, T. Z.; and Finn, C. 2024. Mobile aloha: Learning bimanual mobile manipulation with low-cost whole-body teleoperation. *arXiv preprint arXiv:2401.02117*.

Gong, R.; Huang, J.; Zhao, Y.; Geng, H.; Gao, X.; Wu, Q.; Ai, W.; Zhou, Z.; Terzopoulos, D.; Zhu, S.-C.; et al. 2023. Arnold: A benchmark for language-grounded task learning with continuous states in realistic 3d scenes. In *Proceedings of the IEEE/CVF International Conference on Computer Vision*, 20483–20495.

Grandia, R.; Jenelten, F.; Yang, S.; Farshidian, F.; and Hutter, M. 2023. Perceptive locomotion through nonlinear model-predictive control. *IEEE Transactions on Robotics*, 39(5): 3402–3421.

Gu, Q.; Kuwajerwala, A.; Morin, S.; Jatavallabhula, K. M.; Sen, B.; Agarwal, A.; Rivera, C.; Paul, W.; Ellis, K.; Chellappa, R.; et al. 2024. Conceptgraphs: Open-vocabulary 3d scene graphs for perception and planning. In *2024 IEEE International Conference on Robotics and Automation (ICRA)*, 5021–5028. IEEE.

Ha, H.; Gao, Y.; Fu, Z.; Tan, J.; and Song, S. 2024. Umi on legs: Making manipulation policies mobile with manipulation-centric whole-body controllers. *arXiv preprint arXiv:2407.10353*.

Huang, X.; Huang, Y.-J.; Zhang, Y.; Tian, W.; Feng, R.; Zhang, Y.; Xie, Y.; Li, Y.; and Zhang, L. 2023. Open-set image tagging with multi-grained text supervision. *arXiv preprint arXiv:2310.15200*.

Jatavallabhula, K. M.; Kuwajerwala, A.; Gu, Q.; Omama, M.; Chen, T.; Maalouf, A.; Li, S.; Iyer, G.; Saryazdi, S.; Keetha, N.; et al. 2023. Conceptfusion: Open-set multimodal 3d mapping. *arXiv preprint arXiv:2302.07241*.

Jiang, J.; Zhu, Y.; Wu, Z.; and Song, J. 2025a. DualMap: On-line Open-Vocabulary Semantic Mapping for Natural Language Navigation in Dynamic Changing Scenes. *arXiv preprint arXiv:2506.01950*.

Jiang, Y.; Zhang, R.; Wong, J.; Wang, C.; Ze, Y.; Yin, H.; Gokmen, C.; Song, S.; Wu, J.; and Fei-Fei, L. 2025b. Behavior robot suite: Streamlining real-world whole-body manipulation for everyday household activities. *arXiv preprint arXiv:2503.05652*.

Kim, M. J.; Pertsch, K.; Karamcheti, S.; Xiao, T.; Balakrishna, A.; Nair, S.; Rafailov, R.; Foster, E.; Lam, G.; Sanketi, P.; et al. 2024. Openvla: An open-source vision-language-action model. *arXiv preprint arXiv:2406.09246*.

Liu, M.; Chen, Z.; Cheng, X.; Ji, Y.; Qiu, R.-Z.; Yang, R.; and Wang, X. 2024a. Visual whole-body control for legged loco-manipulation. *arXiv preprint arXiv:2403.16967*.

Liu, P.; Guo, Z.; Warke, M.; Chintala, S.; Paxton, C.; Shafullah, N. M. M.; and Pinto, L. 2024b. Dynamem: Online dynamic spatio-semantic memory for open world mobile manipulation. *arXiv preprint arXiv:2411.04999*.

Mittal, M.; Yu, C.; Yu, Q.; Liu, J.; Rudin, N.; Hoeller, D.; Yuan, J. L.; Singh, R.; Guo, Y.; Mazhar, H.; Mandlekar, A.; Babich, B.; State, G.; Hutter, M.; and Garg, A. 2023. Orbit: A Unified Simulation Framework for Interactive Robot Learning Environments. *IEEE Robotics and Automation Letters*, 8(6): 3740–3747.

Nasiriany, S.; Maddukuri, A.; Zhang, L.; Parikh, A.; Lo, A.; Joshi, A.; Mandlekar, A.; and Zhu, Y. 2024. Robocasa: Large-scale simulation of everyday tasks for generalist robots. *arXiv preprint arXiv:2406.02523*.

Pan, G.; Ben, Q.; Yuan, Z.; Jiang, G.; Ji, Y.; Li, S.; Pang, J.; Liu, H.; and Xu, H. 2025a. RoboDuet: Learning a Cooperative Policy for Whole-body Legged Loco-Manipulation. *IEEE Robotics and Automation Letters*.

Pan, M.; Zhang, J.; Wu, T.; Zhao, Y.; Gao, W.; and Dong, H. 2025b. Omnimaniip: Towards general robotic manipulation via object-centric interaction primitives as spatial constraints. In *Proceedings of the Computer Vision and Pattern Recognition Conference*, 17359–17369.

Qi, Z.; Zhang, W.; Ding, Y.; Dong, R.; Yu, X.; Li, J.; Xu, L.; Li, B.; He, X.; Fan, G.; et al. 2025. Sofar: Language-grounded orientation bridges spatial reasoning and object manipulation. *arXiv preprint arXiv:2502.13143*.

Qiu, R.-Z.; Hu, Y.; Song, Y.; Yang, G.; Fu, Y.; Ye, J.; Mu, J.; Yang, R.; Atanasov, N.; Scherer, S.; et al. 2024a. Learning generalizable feature fields for mobile manipulation. *arXiv preprint arXiv:2403.07563*.

Qiu, R.-Z.; Song, Y.; Peng, X.; Suryadevara, S. A.; Yang, G.; Liu, M.; Ji, M.; Jia, C.; Yang, R.; Zou, X.; et al. 2024b. Wildlma: Long horizon loco-manipulation in the wild. *arXiv preprint arXiv:2411.15131*.

Ren, T.; Liu, S.; Zeng, A.; Lin, J.; Li, K.; Cao, H.; Chen, J.; Huang, X.; Chen, Y.; Yan, F.; Zeng, Z.; Zhang, H.; Li, F.; Yang, J.; Li, H.; Jiang, Q.; and Zhang, L. 2024. Grounded SAM: Assembling Open-World Models for Diverse Visual Tasks. *arXiv:2401.14159*.

Shridhar, M.; Manuelli, L.; and Fox, D. 2022. Perceiver-Actor: A Multi-Task Transformer for Robotic Manipulation. *arXiv:2209.05451*.

Team, G. 2025. GenieSim.

Wang, H.; Chen, J.; Huang, W.; Ben, Q.; Wang, T.; Mi, B.; Huang, T.; Zhao, S.; Chen, Y.; Yang, S.; et al. 2024a. Grutopia: Dream general robots in a city at scale. *arXiv preprint arXiv:2407.10943*.

Wang, J.; Rajabov, J.; Xu, C.; Zheng, Y.; and Wang, H. 2024b. Quadwbg: Generalizable quadrupedal whole-body grasping. *arXiv preprint arXiv:2411.06782*.

Wang, Y.; Zhu, H.; Liu, M.; Yang, J.; Fang, H.-S.; and He, T. 2025. VQ-VLA: Improving Vision-Language-Action Models via Scaling Vector-Quantized Action Tokenizers. *arXiv preprint arXiv:2507.01016*.

Zhang, C.; Han, D.; Zheng, S.; Choi, J.; Kim, T.-H.; and Hong, C. S. 2023. MobileSAMv2: Faster Segment Anything to Everything. *arXiv:2312.09579*.

Zhang, H.; Yu, H.; Zhao, L.; Choi, A.; Bai, Q.; Yang, B.; and Xu, W. 2025. Slim: Sim-to-real legged instructive manipulation via long-horizon visuomotor learning. *arXiv preprint arXiv:2501.09905*.

Zhi, P.; Zhang, Z.; Zhao, Y.; Han, M.; Zhang, Z.; Li, Z.; Jiao, Z.; Jia, B.; and Huang, S. 2024. Closed-loop open-vocabulary mobile manipulation with gpt-4v. *arXiv preprint arXiv:2404.10220*.

Zhou, C.; Loy, C. C.; and Dai, B. 2022. Extract free dense labels from clip. In *European conference on computer vision*, 696–712. Springer.

Zhuang, Z.; Fu, Z.; Wang, J.; Atkeson, C.; Schwertfeger, S.; Finn, C.; and Zhao, H. 2023. Robot parkour learning. *arXiv preprint arXiv:2309.05665*.

Appendix

A Long-horizon Planner Pipeline

A.1 Instance-Level Semantic Graph Construction

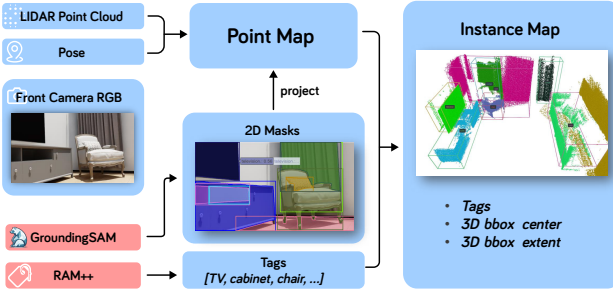


Figure 5: Instance-level graph construct pipeline.

To enable egocentric task planning, we implement an online multi-modal perception pipeline that constructs an instance-level semantic graph from onboard sensors.

A downward-facing LiDAR provides real-time point clouds at 10 Hz, which are aggregated into a global point map using the robot’s estimated pose. This map serves both as a geometric substrate for semantic abstraction and as a SLAM-based 2D occupancy grid for path planning.

In parallel, a front-facing RGB camera captures visual frames. We use RAM++ (Huang et al. 2023) to identify candidate object labels from each RGB image. These labels, along with the image, are fed into Grounding-SAM (Ren et al. 2024) to obtain instance-level segmentation masks m_i . We replace the standard SAM model with Mobile-SAM (Zhang et al. 2023) to improve efficiency. The masks are projected onto the current LiDAR frame to obtain per-object point cloud segments.

Inspired by prior works (Gu et al. 2024; Jatavallabhula et al. 2023), to enable consistent object tracking across time, we fuse observations using both semantic and geometric similarity:

- Semantic Similarity. For each instance mask, we extract a sparse visual-semantic feature map f_I using MaskCLIP (Zhou, Loy, and Dai 2022). We pool features within each mask m_i to generate an instance-level descriptor $\mathbf{f}_i \in \mathbb{R}^d$. Two instances i and j are considered semantically consistent if their cosine similarity satisfies:

$$\text{sim}_{\text{sem}}(\mathbf{f}_i, \mathbf{f}_j) = \frac{\mathbf{f}_i^\top \mathbf{f}_j}{\|\mathbf{f}_i\| \|\mathbf{f}_j\|} > \tau_{\text{sem}}, \quad \tau_{\text{sem}} = 0.8. \quad (9)$$

- Geometric Similarity. Let \mathcal{P}_i and \mathcal{P}_j be the point sets of two object candidates. We consider them geometrically aligned if at least 80% of the points in \mathcal{P}_i have a nearest neighbor in \mathcal{P}_j within radius ϵ :

$$\frac{1}{|\mathcal{P}_i|} \sum_{\mathbf{p} \in \mathcal{P}_i} \mathbb{I} \left[\min_{\mathbf{q} \in \mathcal{P}_j} \|\mathbf{p} - \mathbf{q}\| < \epsilon \right] > \tau_{\text{geo}}, \quad \tau_{\text{geo}} = 0.8. \quad (10)$$

When both criteria are satisfied, the two instances are merged as the same object across time.

The final instance graph $G = \{O_i\}$ contains nodes O_i with attributes including semantic tags and 3D bounding boxes. This symbolic representation serves as the input for downstream task decomposition and decision-making.

A.2 Hierarchical Planning Prompts

LLM-based Task-level Prompts This section illustrates how we leverage large language models (LLMs) to decompose tasks into structured symbolic action sequences (e.g., navigate, pick, place). The prompt input consists of the user instruction and a summarized semantic scene graph. Example prompts are shown in Fig. 10.

VLM-based Manipulation Prompts For the execution of atomic manipulation actions, we demonstrate how vision-language models (VLMs) are used to infer task-relevant contact points and end-effector orientations. The prompt input includes a first-person RGB observation and a natural language description of the current sub-task. Examples are shown in Fig. 11.

B Whole-body Policy Training

B.1 Reward design

This section details the key reward terms used during policy training, summarized in Table 5.

Term	Equation	Weight	
		Stage 1	Stage 2
r_{xy}^{track}	$\exp(-((\hat{\mathbf{v}}_{xy} - \mathbf{v}_{xy})) / \gamma_{xy})$	2.75	2.75
r_{yaw}^{track}	$\exp(-((\hat{\omega} - \omega)) / \gamma_\omega)$	1.50	1.50
$r_{ee-pos}^{\text{track}}$	$\sqrt{(\hat{\mathbf{p}}_{ee} - \mathbf{p}_{ee})^2}$	0.00	-1.20
$r_{ee-ori}^{\text{track}}$	$\sqrt{(\hat{\phi}_{ee} - \phi_{ee})^2}$	0.00	-1.50
r_{gait}	Eq. 17	0.75	0.75
r_{freq}	Eq. 19	1.25e1	1.25e1
r_{base}^{base}	$ \tau_{\text{base}}^{\text{base}} ^2$	-2.0e-4	-2.0e-4
r_{base}^{acc}	$ \dot{\mathbf{q}}_{\text{base}} ^2$	-2.5e-7	-2.0e-7
r_{base}^{power}	$ \tau_{\text{base}}^{\text{base}} * \dot{\mathbf{q}}_{\text{base}} $	-2.0e-5	-2.0e-5
r_{arm}^{base}	$ \tau_{\text{arm}}^{\text{base}} ^2$	0.00	-4.0e-4
r_{arm}^{acc}	$ \dot{\mathbf{q}}_{\text{arm}} ^2$	0.00	-2.5e-6
r_{arm}^{power}	$ \tau_{\text{arm}}^{\text{base}} * \dot{\mathbf{q}}_{\text{arm}} $	0.00	-2.0e-4
r_{smooth}	$\sqrt{(\mathbf{a}_t - \mathbf{a}_{t-1})^2}$	-0.02	-0.02

Table 5: The key reward terms used in policy training

To encourage a stable gait, we use a gait reward r_{gait} that promotes specific foot contact patterns. It encourages synchrony between diagonal leg pairs (FL/RR, FR/RL) using a reward term r_s and asynchrony between all other pairs using r_a . The final gait reward is a multiplicative combination of individual reward terms (r_s, r_a) , which are functions of the squared error between the time two legs (A, B) have spent

in the air (A_{air}) or in contact (A_{cont}).

$$t_{air}^s(A, B) = \text{clip}((A_{air} - B_{air})^2, 0.0, 0.04) \quad (11)$$

$$t_{cont}^s(A, B) = \text{clip}((A_{cont} - B_{cont})^2, 0.0, 0.04) \quad (12)$$

$$r_s(FL, RR) = e^{-(t_{air}^s(FL, RR) + t_{cont}^s(FL, RR))} \quad (13)$$

$$t_{air}^a(A, B) = \text{clip}((A_{air} - B_{cont})^2, 0.0, 0.04) \quad (14)$$

$$t_{cont}^a(A, B) = \text{clip}((A_{cont} - B_{air})^2, 0.0, 0.04) \quad (15)$$

$$r_a(FL, FR) = e^{-(t_{air}^a(FL, FR) + t_{cont}^a(FL, FR))} \quad (16)$$

$$r_{gait} = \prod_{i,j \in \text{sync pairs}} r_s(i, j) \cdot \prod_{k,l \in \text{async pairs}} r_a(k, l) \quad (17)$$

A frequency reward r_{fre} regulates the gait’s cadence by penalizing deviation from a target frequency f_{target} . The frequency for each leg $f(\text{leg})$ is the inverse of the time between consecutive ground contacts ($t_k^{cont} - t_{k-1}^{cont}$), where k is the timestamp. The frequency reward r_{fre} is defined as below:

$$r_f(\text{leg}) = \exp(-0.5 \cdot (f(\text{leg}) - f_{target})^2) \quad (18)$$

$$r_{fre} = \prod_{\text{leg} \in \text{FL,FR,RL,RR}} r_f(\text{leg}) \quad (19)$$

In stage one, training focuses on locomotion. The reward function includes task-specific terms for base velocity tracking ($r_{xy}^{track}, r_{yaw}^{track}$) and gait shaping (r_{gait}, r_{freq}). To improve stability and facilitate sim-to-real transfer, several regularization rewards are applied. These include penalties on torque (r_{torque}), joint acceleration (r_{acc}) and action-to-action changes (r_{smooth}) to encourage stable policy outputs. Additionally, a power consumption penalty (r_{power}) is used to discourage excessive mechanical work. In stage two, all Stage one rewards are retained, and new task-specific terms are introduced for end-effector pose tracking (position $r_{ee_pos}^{track}$ and orientation $r_{ee_ori}^{track}$). Furthermore, the regularization penalties (torque, acceleration, and power) are extended to include the manipulator’s joints.

B.2 Domain randomization

Parameter	Ranges	Method
Friction	[0.4, 2.0]	-
Base Mass	[-5.0, 5.0]	add
Base Pushing	x: [-0.5, 0.5] y: [-0.5, 0.5]	interval
Actuator Gains	[0.8, 1.2]	scale
Ee Link Mass	[0.0, 0.2]	add
Joint reset	[0.5, 1.5]	scale
Base reset	x: [-0.5, 0.5], y: [-0.5, 0.5] ω: [-π, π], v _x : [-0.5, 0.5] v _y : [-0.5, 0.5], v _z : [-0.5, 0.5] α: [-0.5, 0.5], β: [-0.5, 0.5] γ: [-0.5, 0.5]	add

Table 6: The domain randomization ranges. The method means the method of randomization, where “add” means add to the original, “scale” means scale up the original, and “interval” means continue for a while.

To enhance out-of-distribution generalization and facilitate sim-to-real transfer, our policy is trained with extensive domain randomization, as detailed in Table 6. This process includes randomizing the robot’s initial conditions, such as its base pose and joint configuration, at the start of each episode. Crucially, to ensure adaptability to tasks involving different payloads, the mass of the end-effector is also randomized.

C Benchmark Configurations

This section presents the task setup used in our benchmark evaluation, including both short-horizon and long-horizon mobile manipulation tasks.

C.1 ARNOLD Short-Horizon Tasks

To evaluate the fine-grained manipulation capabilities of our system, we migrate four short-horizon tasks from the ARNOLD benchmark into our custom simulation environment. These tasks are designed to assess step-wise visuo-motor precision and generalization under diverse configurations.

Simulation Integration. To enable evaluation within our own simulation platform, we convert the raw ARNOLD data into standardized YAML configuration files. The conversion pipeline involves:

1. Parsing each .npz sample to extract task-specific parameters, including scene setup, object category, pose, and robot initial state.
2. Transforming all coordinate frames from ARNOLD’s convention to that of our simulator.
3. Automatically generating natural language task instructions and adjusting the robot’s initial pose to ensure reachability and feasibility.
4. Grouping tasks by scene and saving them as per-scene YAML files containing layout, object initialization, evaluation metrics, and interaction constraints.

This setup ensures consistent large-scale deployment and reproducible benchmarking of ODYSSEY’s short-horizon manipulation performance across multiple scenarios. Examples of multiple tasks sharing a single scene configuration are shown in Figure 6.

Action Sequence Structure. To facilitate scalable benchmarking, we adopt predefined action sequences in place of LLM-based task decomposition. This ensures consistent execution patterns across trials and enables focused evaluation of local manipulation accuracy independent of high-level planning variance. For instance, the OPENCABINET task consists of the following four phases:

- **Observe & Plan:** Capture the scene (o_1) to identify the semantic target and compute the desired end-effector pose a^* for contact.
- **Pre-Alignment:** Move the gripper to a pre-contact pose located 10 cm away from a^* along the approach axis (opposite to gripper’s z -axis).

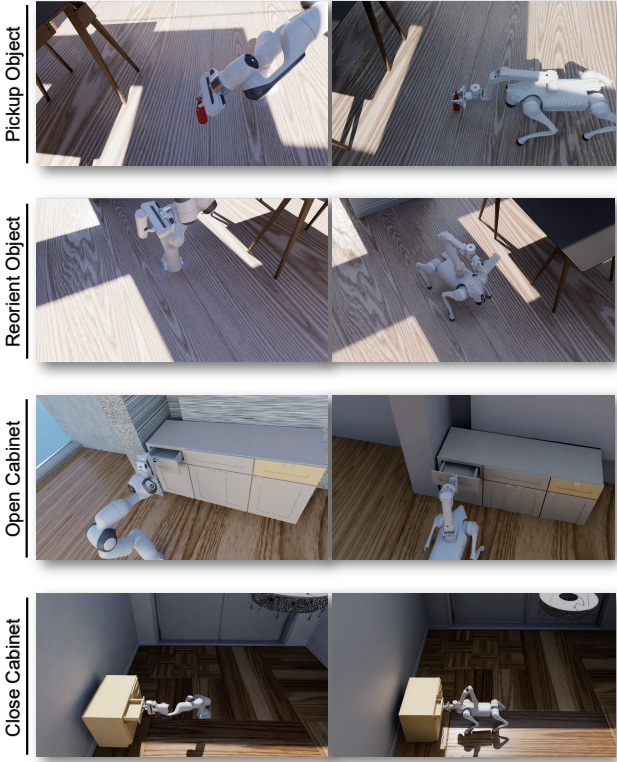


Figure 6: ARNOLD converted environments of four tasks.

- **Execute Grasp:** Linearly advance the gripper along the approach direction to reach a^* and close the fingers to secure the object.
- **Task Completion:** Apply the task-specific motion (e.g., pulling, lifting) until the environment state satisfies the success condition.

This structured formulation allows for fine-grained progress monitoring at 0%, 33%, 66%, and 100% completion stages, as illustrated in Figure 7.

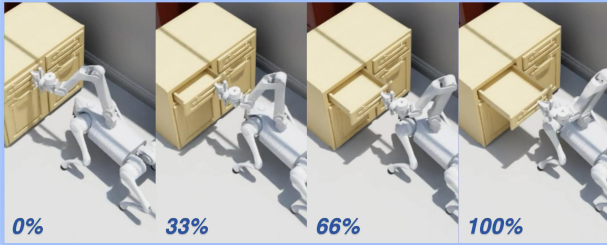


Figure 7: The continuous state monitoring of ARNOLD short-horizon tasks.

C.2 ODYSSEY Long-Horizon Tasks

As shown in Fig. 8. Our benchmark includes eight long-horizon tasks constructed to evaluate full-pipeline perfor-

mance, spanning perception, task planning, navigation, and manipulation. Each task consists of 2–3 subgoals and is designed with diverse object types, spatial distributions, and physical interaction modes.

Table 7 summarizes the tasks, listing the task name, number of variations, and number of unique asset types involved in each.

Task Names	Variations	Assets
INDOORCOLLECT	45	65
ROOMNAVIGATION	43	11
CARTDELIVERY	39	47
CABINETSTORAGE	49	69
RESTOCKING	30	34
SHOPPING	40	45
OUTDOORCOLLECT	30	47
OUTDOORDELIVERY	28	48

Table 7: Overview of 8 long-horizon tasks with names, variation counts, and asset usage per task.



Figure 8: ODYSSEY benchmark details. Including task type, scene, and object configuration details.

D Experiment Details

D.1 Short-Horizon Evaluation

Data Split To assess generalization under various task variations, the ARNOLD benchmark defines five splits:

- **Test:** All components—objects, scenes, and states—are seen during training.
- **Novel Object:** Involves unseen objects, with seen scenes and goal states.
- **Novel Scene:** Uses unseen environments while keeping objects and goals seen.
- **Novel State:** Includes novel goal configurations under seen objects and scenes.
- **Any State:** Targets fine-grained generalization to arbitrary continuous goals.

In Section 4.1, we report the average success rate over the last four splits as a unified **Novel** setting for simplicity and comparison clarity. Here in the appendix, we present detailed breakdowns across all five splits.

Baselines and Evaluation Protocol In Section 4.1, we primarily compare ODYSSEY with PerAct, the strongest baseline from ARNOLD. For a more complete analysis, we extend the evaluation to include all three PerAct variants:

- **PerAct:** The standard model based on voxelized RGB-D fusion and Perceiver Transformer.

- **PerAct[†]:** Enhanced with value-function supervision to improve decision-making.

- **PerAct (MT)[†]:** A multi-task trained variant leveraging more diverse training signals.

In addition, following the ARNOLD evaluation protocol, each model is evaluated in a two-phase setup:

- **Phase I (End-to-End):** Includes both grasping and subsequent manipulation.

- **Phase II (Manipulation Only):** Uses ground-truth grasp poses to isolate manipulation performance.

This extended evaluation reveals the specific strengths and failure modes of ODYSSEY compared to baselines, particularly under generalization stress tests.

Results and Failure Analysis Table 8 presents detailed performance across all tasks and data splits. ODYSSEY consistently outperforms all PerAct variants, particularly in generalization settings involving novel objects, scenes, or goal states. The two-phase evaluation further highlights the robustness of our manipulation module when decoupled from grasping errors.

Common failure cases across tasks are largely attributed to (1) inaccurate semantic reasoning by the vision-language model (VLM), such as object orientation confusion or sub-optimal contact point prediction, and (2) challenges in physical interaction execution, including occlusion, narrow geometry, and unstable force transfer.

- **PICKUPOBJECT**: Phase I failures mainly arise from misjudged object orientation or selecting hard-to-grasp regions (e.g., bottlenecks). These issues are largely resolved in phase II, validating the effectiveness of our pose-conditioned manipulation.
- **REORIENTOBJECT**: Errors stem from inaccurate initial pose estimation or weak grasps on thin sections, leading to slippage during reorientation. ODYSSEY exhibits robust generalization even under such dynamic conditions.
- **OPENCABINET**: Limited improvement in phase II suggests inherent difficulty in the manipulation itself. Failures often relate to misidentified handles, drawer confusion, or inaccurate grasp positioning.
- **CLOSECABINET**: Performance is mainly affected by occlusion and poor camera framing. Handles are sometimes out of view during approach or are visually ambiguous due to lighting or textures.

In summary, ODYSSEY demonstrates strong semantic grounding, generalization, and precision control, particularly in high-complexity tasks. Remaining challenges highlight future directions in visual robustness and contact policy refinement.

D.2 Long-Horizon Evaluation

Failure Analysis To complement the long-horizon evaluation in Section 4.1, we present a failure mode analysis aggregated over all 6 indoor and 2 outdoor ODYSSEY tasks. Rather than reporting per-task breakdowns, we group failures by environment type and visualize them separately for indoor and outdoor scenarios.

Each failure is assigned to one of the following three categories:

- **Reasoning Failure**: Errors arising from the LLM-based task planner or VLM-based local action advisor, including incorrect subgoal decomposition, ambiguous symbolic grounding, or mispredicted contact poses.
- **Control Failure**: Low-level execution issues related to either locomotion or manipulation, such as unstable whole-body control on uneven terrain or failed grasp execution due to poor alignment or force instability.
- **Navigation Failure**: Failures caused by inability to bring target objects into a feasible manipulation workspace, or collisions during path execution due to inaccurate waypoint planning or obstacle avoidance.

Figure 9 shows the distribution of these failure types across indoor and outdoor tasks. From the analysis, we draw several key observations:

- **Indoor tasks are dominated by reasoning and control failures.** Tasks such as CABINETSTORAGE and RESTOCKING, which involve complex semantic reasoning

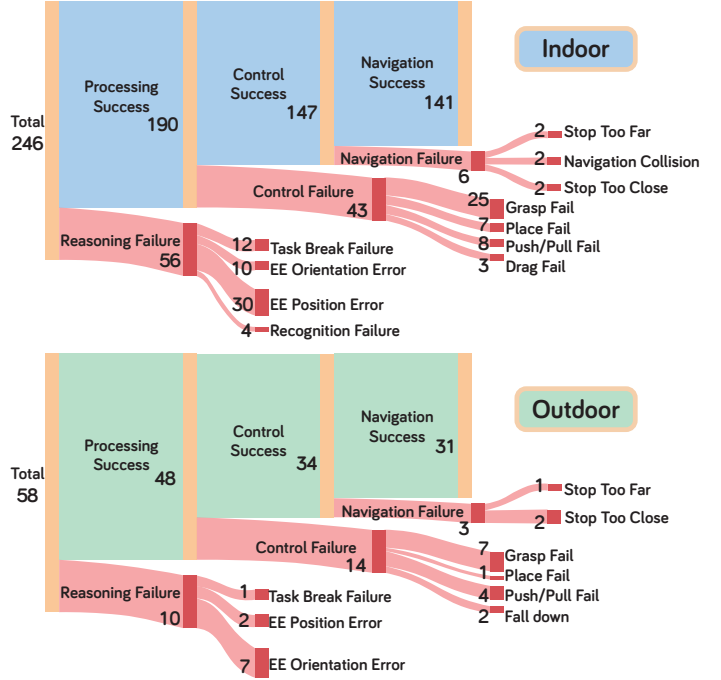


Figure 9: **Failure breakdown by environment type.** Failures are categorized into reasoning, control, and navigation errors. Indoor tasks suffer more from language and control failures, while navigation becomes more challenging in outdoor scenarios.

and precise manipulation, frequently fail due to incorrect subgoal decomposition or inaccurate contact prediction. Control-related issues, such as unstable grasps and force misalignment, are also prevalent due to tight spatial constraints and object diversity in indoor environments.

- **Control failures in outdoor scenarios are often tied to whole-body instability.** Unlike indoors, where control issues center on gripper-object interaction, outdoor control failures are more frequently caused by the robot falling or losing balance, particularly during manipulation actions performed on slopes or uneven surfaces.
- **Reasoning errors span both global and local levels.** Global planning failures include incorrect symbolic grounding or subgoal ordering, while local failures stem from misidentifying contact points or failing to detect objects due to occlusions or poor lighting.

Split	Method	PICKUPOBJECT	REORIENTOBJECT	OPENCABINET	CLOSECABINET		
Test	PerAct	94.03	97.76	19.48	24.68	24.64	42.03
	PerAct \dagger	94.78	95.52	24.68	28.57	23.19	49.28
	PerAct (MT) \dagger	90.30	92.54	14.29	20.78	20.29	39.13
	ODYSSEY	60.45	81.34	51.32	76.32	56.30	64.70
Novel Object	PerAct	86.55	92.73	11.40	35.09	0.00	0.00
	PerAct \dagger	87.27	91.27	10.53	32.46	0.00	4.94
	PerAct (MT) \dagger	81.09	85.45	7.89	24.56	0.00	4.94
	ODYSSEY	41.09	72.36	31.58	64.04	50.32	61.29
Novel Scene	PerAct	72.85	84.62	17.07	31.71	0.00	4.97
	PerAct \dagger	69.68	84.16	13.41	37.80	0.55	4.97
	PerAct (MT) \dagger	67.87	79.64	7.32	29.27	1.10	4.42
	ODYSSEY	43.43	63.80	41.98	54.32	52.94	64.31
Novel State	PerAct	2.38	0.68	0.00	0.95	0.00	5.81
	PerAct \dagger	0.68	2.38	0.48	0.00	0.00	6.22
	PerAct (MT) \dagger	2.04	3.06	0.95	2.38	0.00	3.73
	ODYSSEY	46.60	78.91	67.48	81.07	48.85	63.22
Any State	PerAct	47.01	50.75	7.79	19.48	5.80	21.74
	PerAct \dagger	48.51	47.76	14.29	14.29	4.35	24.64
	PerAct (MT) \dagger	46.27	47.01	12.99	12.99	4.35	5.80
	ODYSSEY	47.22	80.59	51.95	81.82	54.78	67.83

Table 8: **Evaluation results across short-horizon tasks and data splits.** Each row corresponds to a specific split, and each column reports success rates (%) on a task. Gray entries denote phase-II performance using ground-truth grasp poses. ODYSSEY outperforms all PerAct variants, especially in generalization and manipulation settings.

[System Prompt]

You are a quadruped robot with a robotic arm that needs to understand 3D scene graphs to complete task planning.

Input Information

3D Scene Graph: JSON format describing scene objects and robot itself, where each object contains:

- "object_tag": Brief tags categorizing the object (sometimes inaccurate)
- "bbox_extent": Extents of the 3D bounding box for the object in x, y, z direction
- "bbox_center": Centroid of the 3D bounding box for the object

Task Requirements

When given a task description, you need to:

1. **Task Decomposition:** Break down complex sequential tasks into a series of atomic actions

2. **Action Types:** Only use these predefined atomic actions:

- "nav": Navigate to a position
- "pick": Pick up an object
- "place": Place a held object
- "pull": Pull an articulated object while the quadruped remains stationary.
- "push": Push an articulated object while the quadruped remains stationary.
- "drag": Drag an object along the ground to a target location while the quadruped walks with it.

Output Format

Respond with a JSON array (enclosed in a Markdown fenced code) of actions, where each action is a dictionary containing:

```
```json {
 "inferred_query": "Your interpretation of this specific action",
 "action_type": "One of [nav, pick, place, pull, push, drag]",
 "relevant_object": "the most relevant object name robot need to locate for this action (if applicable)",
 "query_achievable": "Boolean - whether this action is achievable using the objects in the 3D scene",
 "target_pose": [x, y], // Only for nav/drag actions: center of target object in 2D Map
} ```
```

## [User]

Task: {text} Scene JSON: {scene\_graph} Robot current pose (x, y, yaw): {robot\_pose}

Figure 10: Prompt examples for task-level planning using LLM. The model is conditioned on a semantic instance graph and a goal instruction, and produces a structured list of atomic actions.

### [Position System Prompt]

You are a robot assistant. Below is an RGB image (size:640\*480) taken from a camera on the robot's gripper. Once you have the image the user will enter a task description. Then you need to respond with a JSON dictionary with the following fields:

1. "inferred\_query": your interpretation of the user query in a succinct form
2. "relevant\_object": the most relevant object or part name which robot need to interact in current action
3. "query\_achievable": whether or not the user specified query is achievable according to current view
4. "explanation": first describe the object's spatial relationship to the environment and its pose/orientation (e.g., standing upright, lying flat, tilted, facing direction), then explain how you determined the final guide orientation.
5. "guide\_point": pixel coordinate [x, y] which guide the gripper center where to reach.
6. "place\_type": only include this for place actions. The value must be either "container" or "platform" based on the nature of the placement target.

#### TIPS:

When try to place an object, do not set the guide point at the held object but at where to place.  
Adjust the guide point to a visible region if the target point is occluded by other objects.

### [Orientation System Prompt]

You are a robot assistant. Based on the camera image and a task description, analyze key geometric information and output a JSON dictionary with the following fields:

1. "reasoning": A brief summary of your analysis.
2. "task\_type":
  - "is\_object\_only": 1 if the task involves only object geometry.
  - "is\_object\_and\_surface": 1 if both object and surface are relevant.
3. "object\_analysis":
  - "has\_principal\_axis": 1 if the object has a dominant long axis.
  - "principal\_axis\_angle": Angle of this axis in degrees (-90 to 90). Horizontal = 0°, vertical = 90°.
4. "surface\_analysis":
  - "is\_relevant": 1 if the surface is relevant to the task.
  - "normal\_is\_vertical": 1 if the surface normal is vertical.
  - "normal\_is\_horizontal": 1 if the surface normal is horizontal.

### [User]

Task description: “ **Pick up the toy gun.**”

### [Result]

guide\_point: [290, 275]  
parsed\_orientation: [45, -90, 0]



Figure 11: Prompt examples for local manipulation guidance using VLM. Given an egocentric image and sub-task description, the model predicts a contact point and end-effector orientation under geometric constraints.